REPORT DOCUMENTATION PAGE

Form Approved
OMB No. 0704-0188

1. REPORT DATE *(DD-MM-YYYY)*	**2. REPORT TYPE**	**3. DATES COVERED** *(From - To)*
February 2013	Technical Paper	February 2013-May 2013

4. TITLE AND SUBTITLE
Comprehensive Fuel Spray Modeling and Impacts on Chamber Acoustics in Combustion Dynamics Simulations

5a. CONTRACT NUMBER
In-House

5b. GRANT NUMBER

5c. PROGRAM ELEMENT NUMBER

6. AUTHOR(S)
Yoon, C., Gejji, R., Anderson, W. and Sankaran, V.

5d. PROJECT NUMBER

5e. TASK NUMBER

5f. WORK UNIT NUMBER
3002125K

7. PERFORMING ORGANIZATION NAME(S) AND ADDRESS(ES)

Air Force Research Laboratory (AFMC)
AFRL/RQR
5 Pollux Dr.
Edwards AFB CA 93524-7048

8. PERFORMING ORGANIZATION REPORT NO.

9. SPONSORING / MONITORING AGENCY NAME(S) AND ADDRESS(ES)
Air Force Research Laboratory (AFMC)
AFRL/RQR
5 Pollux Drive
Edwards AFB CA 93524-7048

10. SPONSOR/MONITOR'S ACRONYM(S)

11. SPONSOR/MONITOR'S REPORT NUMBER(S)
AFRL-RQ-ED-TP-2013-044

12. DISTRIBUTION / AVAILABILITY STATEMENT
Distribution A: Approved for Public Release; Distribution Unlimited. PA#13184

13. SUPPLEMENTARY NOTES
Conference paper for the ILASS Americas, 25th Annual Conference on Liquid Atomization and Spray Systems, Pittsburgh, PA, 5-8 May 2013.

14. ABSTRACT
The current study focuses on comprehensive fuel spray modeling and its effects on chamber acoustics in combustion dynamics simulations. The fuel spray is modeled using an Eulerian-Lagrangian approach describing the atomizer internal flow, primary atomization, and secondary atomization processes. To anchor the fuel spray model, a series of experiments has been conducted on the fuel atomizer with and without co-owing air. Spray cone angle, drop-size and velocity distributions were obtained using a high speed camera and Phase Doppler Anemometry (PDA). The fuel spray model results show reasonable agreement with the measured spray cone angles. The computed drop size and velocity distribution however indicate some discrepancies compared with the experimental results suggesting model limitations in describing secondary atomization. In addition, effects of fuel spray modeling on chamber acoustics are studied using combustion dynamics simulations. Three fuel spray models specified drop size distribution, single droplet injection and hollow-cone injection--have been used. Among the three models, the hollow cone injected fuel spray shows good qualitative comparison of chamber acoustics with the experimental results. The pressure fluctuation amplitudes from the simulation, however, underestimate the measured amplitudes. Insufficient description of secondary atomization in the spray model appears to be a critical factor that leads to the observed discrepancies in the fuel spray and combustion dynamics simulations.

15. SUBJECT TERMS

16. SECURITY CLASSIFICATION OF:			**17. LIMITATION OF ABSTRACT**	**18. NUMBER OF PAGES**	**19a. NAME OF RESPONSIBLE PERSON**
					Shawn Phillips
a. REPORT	**b. ABSTRACT**	**c. THIS PAGE**			**19b. TELEPHONE NO** *(include area code)*
Unclassified	**Unclassified**	**Unclassified**	SAR	16	661-525-5621

Standard Form 298 (Rev. 8-98)
Prescribed by ANSI Std. 239.18

ILASS-Americas 25th Annual Conference on Liquid Atomization and Spray Systems, Pittsburgh, PA, May 2013

Comprehensive Fuel Spray Modeling and Impacts on Chamber Acoustics in Combustion Dynamics Simulations

Changjin Yoon, Rohan Gejji, and William E. Anderson*
Maurice J. Zucrow Laboratories
Purdue University
West Lafayette, IN 47907 USA

and

Venkateswaran Sankaran
Propulsion Directorate
Air Force Research Laboratory
Edwards AFB, CA 93524

Abstract

The current study focuses on comprehensive fuel spray modeling and its effects on chamber acoustics in combustion dynamics simulations. The fuel spray is modeled using an Eulerian-Lagrangian approach describing the atomizer internal flow, primary atomization, and secondary atomization processes. To anchor the fuel spray model, a series of experiments has been conducted on the fuel atomizer with and without co-flowing air. Spray cone angle, drop-size and velocity distributions were obtained using a high speed camera and Phase Doppler Anemometry (PDA). The fuel spray model results show reasonable agreement with the measured spray cone angles. The computed drop size and velocity distribution however indicate some discrepancies compared with the experimental results suggesting model limitations in describing secondary atomization. In addition, effects of fuel spray modeling on chamber acoustics are studied using combustion dynamics simulations. Three fuel spray models—specified drop size distribution, single droplet injection and hollow-cone injection—have been used. Among the three models, the hollow cone injected fuel spray shows good qualitative comparison of chamber acoustics with the experimental results. The pressure fluctuation amplitudes from the simulation, however, underestimate the measured amplitudes. Insufficient description of secondary atomization in the spray model appears to be a critical factor that leads to the observed discrepancies in the fuel spray and combustion dynamics simulations.

*Corresponding Author: wanderso@purdue.edu

Introduction

Lean Direct Injection (LDI) is a promising design concept for low-emission gas turbine combustors. In this concept, the liquid fuel is directly injected into the flame zone, and is quickly atomized, mixed, vaporized and reacted with the air within the shortest length and time-scales possible. The LDI-fed combustor is operated under fuel-lean conditions to reduce the overall flame temperatures and consequently to minimize thermal NOx formation. Also, this design inherently precludes the chance of auto-ignition and flashback, which frequently appear in advanced high pressure ratio engines.

The characteristics of the fuel spray is a key factor in LDI engine performance and stability. In the absence of pre-vaporized fuel and premixing with the incoming air, good atomization of the fuel and rapid and uniform mixing with the air are essential for low dry NOx emissions and efficient combustion. Local high flame temperatures leading to undesirable NOx formation can result if the fuel spray is not uniformly distributed. Furthermore, the heat addition into the combustor is directly associated with the fuel spray pattern. If the unsteady heat release induced by fuel spray is in phase with the chamber acoustics, combustion instabilities may arise resulting in potential structural damage of the combustor components and large amounts of NOx emissions. In fact, the LDI design can be more susceptible to thermoacoustic instabilities. Since the LDI engine is operated at fuel-lean conditions, the chemical kinetics and flame surface are more sensitive to disturbances. Consequently, the unsteady heat release can oscillate and lean blowout can occur if there is a significant level of local equivalence ratio fluctuation due to non-uniform mixing or acoustic disturbances.

The emission and flow characteristics of the LDI combustor has been characterized experimentally by several research groups. Tacina et al. (1990) [1] reported NOx emissions from LDI-fed gas turbine combustors and reported results similar to lean-premixed gas turbine combustors. They also characterized the fuel-air mixing in LDI combustors and compared it to relevant pre-atomized spray results. Fu et al. [2] characterized non-reacting spray behavior in LDI configurations using PDA, LDV and 3-D PIV using multiple swirler configurations and fuel injector locations at atmospheric pressure conditions. Both single-element and multiple-element LDI configurations were tested and drop-size and velocities in the spray were measured. A strong relationship was observed between the spray behavior and the swirl number, Reynolds' number and injector location in the LDI element. Besides the multi-phase flow characteristics, several experimental studies have also considered combustion instabilities in LDI-based combustors. Santavicca et al. [3] reported self-excited longitudinal mode combustion dynamics in an optically accessible LDI combustor. Half-wave and full-wave longitudinal mode combustion instabilities were seen to be excited in the combustor at pressure amplitudes of 5-7% of the mean chamber pressure. Most of the heat release from the combustion was found to be in a narrow region downstream of the fuel injector on account of a stable and compact precessing vortex core. Recent experiments conducted by the Purdue group have also reported longitudinal mode combustion instabilities up to 5% of the mean chamber pressure using multiple combustor configurations and equivalence ratios [4]. A brief description of the Purdue combustor and experiments is provided in a later section of this paper.

A pressure-swirl atomizer has been used in the current work. Extensive experimental and computational literature exists that has characterized the internal and external flow through various pressure-swirl atomizer configurations. Jeng et al. [5] studied the liquid sheet emanating from a simplex pressure-swirl atomizer using both computations and experiments and found good agreement between them. An arbitrary Lagrangian-Eulerian numerical method was employed for the computations. Experimental validation was performed using an optically accessible injector and flow visualization was done using a CCD camera. Cousin et al. [6] measured drop-sizes in a pressure swirl atomizer using a Malvern particle-sizer and compared it to results using a theoretical formulation based on the maximization of entropy and reported good agreement.

Computational studies of LDI combustor flows have been conducted by several groups using Lagrangian fuel spray modeling injected from a pressure-swirl atomizer. These studies have focused primarily on the flow characteristics of spray combustion. Patel and Menon's study [7] employed large eddy simulations (LES) with an atomizing spray described by Reitz's Kelvin-Helmholtz (KH) breakup model [8, 9] using single drop injection. The LES results showed the flow characteristics for atomizing and non-atomizing fuel sprays as well as the presence of precessing vortex core instabilities near the LDI element. Consequently, they concluded that the unsteady flow structures and atomization play a significant role in distributing the fuel spray uniformly and widely. Dewanji et al. [10] used the KH breakup model for their multipoint LDI combustor simulations. In their work, injected drops were

atomized as soon as the drop was exposed to the swirling flow and the Sauter Mean Diameter (SMD) of the resulting broken drops near the LDI element ranged from 18 to 22 micron. El-Asrag et al. [11] analyzed combustor flows using a flamelet/progress variable approach with Stanford CDP code and reported that the recirculation bubble structure in the combustor head can be altered by the heat release. Furthermore, Senoner et al. [12] compared computational results from the Stanford CDP and the CERFACS AVBP codes. They specified the fuel injection conditions from empirical relations and no atomization process was modeled. Their results showed that both the Eulerian-Lagrangian approach and the Eulerian-Eulerian approach can provide reasonable predictions of the measured axial velocity profiles.

The present study aims to investigate the effects of fuel spray on the chamber acoustics in a LDI gas turbine combustor. First, the fuel spray is modeled by a comprehensive approach that accounts for the atomizer internal flow, primary and secondary atomization. Next, experimental measurements are conducted to characterize the fuel spray and to validate and guide the development of the computational fuel spray model. For this purpose, a series of non-reacting and atomizing sprays, with and without co-flowing air, are studied experimentally and computationally. Finally, computations and experiments of reacting sprays are used to characterize thermoacoustic instabilities in the LDI gas turbine combustor.

Fuel Spray Modeling

The fuel spray model in the present study aims to describe the key physical processes during the spray breakup as shown in Fig. 1. The spray breakup process can be simplified into three major mechanisms: atomizer internal flow, primary and secondary atomization. In the current study, the atomizer internal flow is computed independently by an Eulerian Volume-Of-Fluid (VOF) method and its results are utilized to describe the Lagrangian spray drop injection. Specifically, the exit flow information from the atomizer flow analysis serves as the initial condition for the spray injection using the hollow-cone injection model. Here, the spray drop size is determined by the liquid film thickness at the orifice exit which is based on the assumption that the liquid film disintegrates into spherical drops. These broken drops can further undergo secondary atomization due to strong inertial and aerodynamic forces. The drop vaporization takes place during the entire process and atomization can contribute to faster vaporization because of the increased total wetted area.

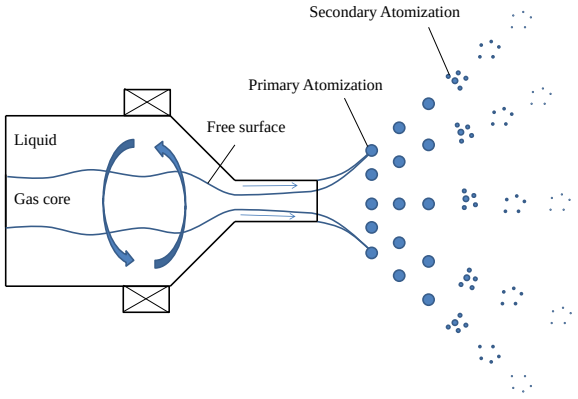

Figure 1. Lagrangian phase events during the spray breakup process

The spray computations reported here except for the atomizer internal flow are carried out with our in-house research code GEMS (General Equation and Mesh Solver) [13]. GEMS solves the Eulerian-phase governing equations using a dual-time implicit scheme that is second-order accurate in time and space. Governing equations for the Eulerian phase consist of the continuity, momentum, energy, turbulence and species conservation equations. Turbulence motions are described by a hybrid RANS/LES method using a length scale modification based on Wilcox's $k-\omega$ two-equation model. [14, 15, 16]. The Lagrangian phase equations are coupled with the Eulerian phase through a source vector. Vaporization is described by the classical D^2-law and, for the chemistry, Westbrook's simplified 2-step global reaction for kerosene/air is assumed [17]. Further details are given in Ref. [4]. The rest of this section describes the Lagrangian modeling of the spray breakup process.

Atomizer Internal Flow Model

Separate computations of the atomizer internal flow are used to provide the spray injection conditions for the fuel spray. The atomizer geometry used in the present study is shown in Fig. 2. Evidently, it is too complicated to describe with an analytical model. For this reason, Ibrahim and Jog's numerical model [18] is employed here. This model is based on a 2D axisymmetric approximation of the geometry, for which the liquid film thickness, spray angle and discharge coefficient have been reported to be within 3 % error compared with experimental measurements. The two-phase flow in the atomizer is described by the Eulerian VOF method using FLU-

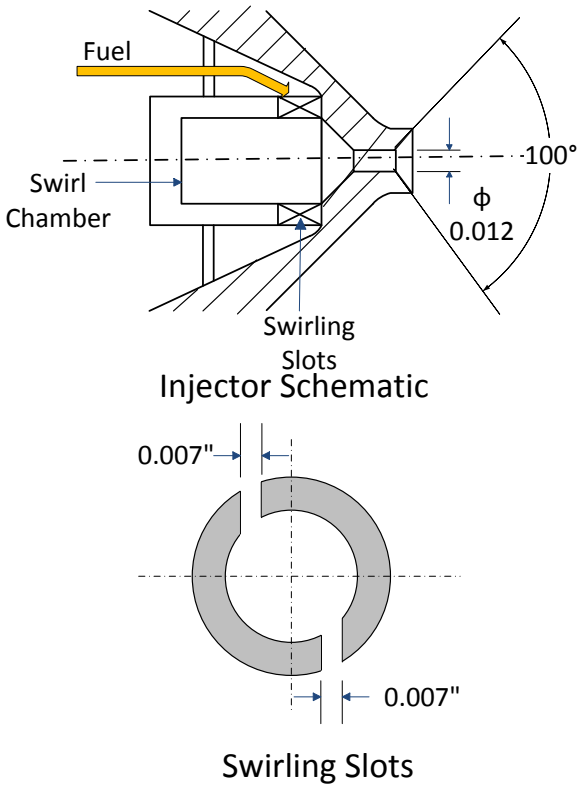

Figure 2. Design of the atomizater

ENT. Reynolds Stress Model (RSM) is used for turbulence closure of the strongly swirling flow in the atomizer. Boundary conditions are indicated along with the computational grid in Fig. 3.

The swirling slots in the atomizer are located at a downstream location in the vortex chamber just before the converging section, unlike in a conventional simplex atomizer in which the swirling ports are located at the vortex chamber head. Due to the axisymmetric approximation, the incoming radial and swirl velocity components are written as:

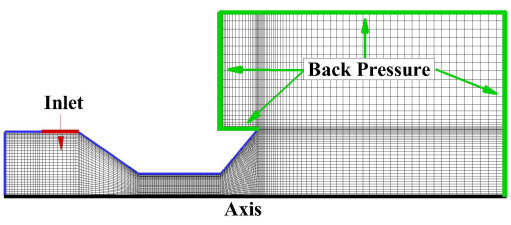

Figure 3. Computational grid and boundary conditions for atomizer internal flow analysis

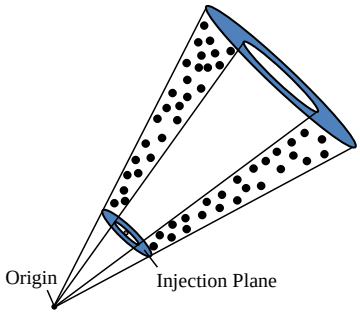

Figure 4. Schematic of hollow cone injection model

$$V_r = \frac{\dot{m}}{2\pi D_c L_s} \tag{1}$$

$$V_\theta = \sqrt{\left(\frac{\dot{m}}{\rho N A_s}\right)^2 - {V_r}^2} \tag{2}$$

where A_s and N are the slot area and the number of slots respectively. In the LDI experiments, the equivalence ratio is controlled by varying the fuel mass flow rate and fixing the air flow rate. For this reason, the radial and swirl components of velocities used for the model inputs can be expressed in term of the equivalence ratio.

Hollow Cone Injection Method

Major parameters taken from the atomizer analysis are the liquid film thickness, velocity vector and spray angle at the atomizer exit plane. Spray drop size at the injection location is approximated by the liquid film thickness and the spray drop is injected using the given velocity components.

The spray produced by pressure swirl atomizer is assumed to be a hollow cone as shown in Fig. 4. The spray cone is defined by the ray origin and annular injection plane. The annulus here is defined by the center of the plane, and inner and outer radius. The spray drops are randomly generated within the given injection plane and its velocity vector is determined by the orientation angle from the origin and angular velocity component. The location where the liquid film is disintegrated (see Fig. 4) is employed for the injection plane.

Secondary Atomization Model

Secondary atomization is modeled by Reitz's breakup model. [8, 9] According to Patel and Menon's study, this model exhibits better accuracy than other existing models in LDI combustor environments. The atomization process in Reitz's model is simulated based on Kelvin-Helmholtz instability

and results of the linear stability analysis are directly used for determining the important atomization parameters. For easier use of the linear stability results, the maximum growth rate, Ω, and corresponding wavelength, λ, of the Kelvin-Helmholtz instability mode are expressed by curve-fits in terms of nondimensional numbers as follows:

$$\Omega\left[\frac{\rho_l a^3}{\sigma}\right]^{0.5} = \frac{\left(0.34 + 0.38\mathrm{We_g}^2\right)}{\left(1+\mathrm{Oh}\right)\left(1+1.4\mathrm{Ta}^{0.6}\right)} \tag{3}$$

$$\frac{\Lambda}{a} = 9.02\frac{\left(1+0.45\mathrm{Oh}^{0.5}\right)\left(1+0.4\mathrm{Ta}^{0.7}\right)}{\left(1+0.87\mathrm{We_g}^{1.67}\right)^{0.6}} \tag{4}$$

where $\mathrm{We_g}$ is the Weber number for the gas phase, $\mathrm{We_g} = \frac{\rho|\mathbf{U}-\mathbf{V}|^2 d}{\sigma}$, Oh is the Ohnesorge number, $\mathrm{Oh} = \nu_1\sqrt{\frac{\rho_l}{\sigma a}}$ and Ta is the Taylor parameter, $\mathrm{Ta} = \mathrm{Oh}\sqrt{\mathrm{We_g}}$. The liquid breakup is modeled by adding new child parcels and their size is determined by

$$r = \begin{cases} B_0\Lambda & (B_0\Lambda \le a) \\ \min\left[\begin{array}{c}\left(3\pi a^2\left|\mathbf{U}-\mathbf{V}\right|/2\Omega\right)^{0.33} \\ \left(3a^2\Lambda/4\right)^{0.33}\end{array}\right] & (B_0\Lambda > a) \end{cases} \tag{5}$$

where B_0 is a model constant and set equal to 0.61. Simultaneously, the parent drop size is reduced by

$$\frac{da}{dt} = -\frac{(a-r)}{\tau} \tag{6}$$

where τ is a time constant and determined from

$$\tau = 3.726 B_1 a/\Lambda\Omega \tag{7}$$

where the model coefficient, B_1 is recommended to be 10 by Reitz [8] and 2 by Patel and Menon. [7] Child parcels are released when the stripped mass removed from the parent parcel exceeds a few percent of the average injected parcel mass. Newly formed parcels have a random velocity direction within a confined cone angle defined by

$$\tan\left(\theta/2\right) = A_1\Lambda\Omega/U \tag{8}$$

where $A_1 = 0.188$. In addition, while the parent parcel reduces, its mass is preserved by controlling the drop numbers contained within a parcel, i.e., $Na^3 = N_0 a_0^3$.

Experimental Setup for Spray Characterization

A pressure swirl atomizer (FN = 1.32) obtained from Woodward (Fig. 2) has been used for the spray characterization tests. Phase Doppler Anemometry (PDA) and high speed videos are used to characterize drop sizes, velocities, and spray cone angle.

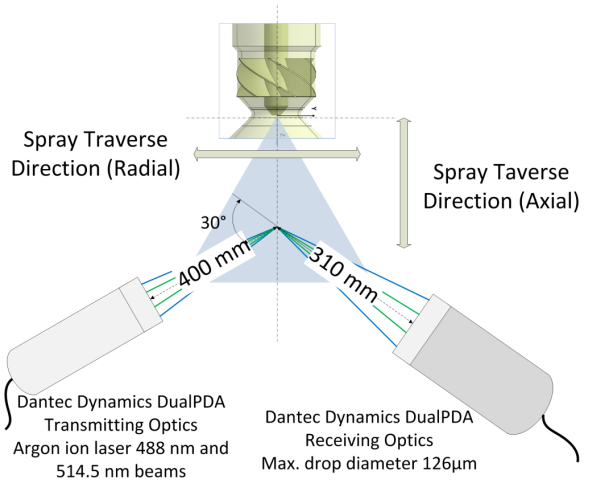

Figure 5. Schematic diagram of PDA test arrangement

For the spray, the fuel flow rate is maintained at the same values as the spray combustion experiments for equivalence ratios of 0.4, 0.5, and 0.6. The spray tests are performed at atmospheric pressure with and without a co-flow of air around the fuel injector. The fuel flow rate is measured across a cavitating venturi (0.025" throat diameter) and verified based on the pressure differential across the injector. For experiments with co-flow of air, the air flow rate is regulated to maintain a $\Delta P/P$ of 4% across the injector which is similar to the values measured in the spray combustion experiments. The co-flowing air passes through a swirler and subsonic venturi. The swirler has six helical axial vanes with a lead angle of 60° yielding a swirl number of approximately 0.8. A schematic diagram of the test arrangement is shown in Fig. 5.

Drop sizes and velocities are recorded with a PDA. The PDA determines the velocity of individual particles based on the frequency shift of light which is reflected or refracted by a moving particle. Drop size is estimated by comparing the phase shift between two detectors at known locations. For the results reported here, a Dantec Dynamics Dual-PDA system was utilized. This system uses an argon-ion laser, beam splitter (514.5 and 488.0 nm wavelengths), and transmitter (400 mm focal length) to create orthogonal measurement volumes for simultaneous recording of two velocity components. The receiver (310 mm focal length) was placed at a scattering angle of 45 degrees, resulting in a theoretical maximum detectable drop diameter of 126 μm, as reported by the PDA software (BSA Flow Software version 4.00.00.42). To capture the local statis-

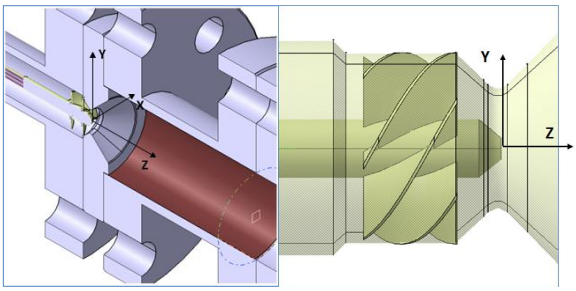

Figure 7. Schematic diagram of the fuel-injector-swirler-venturi configuration

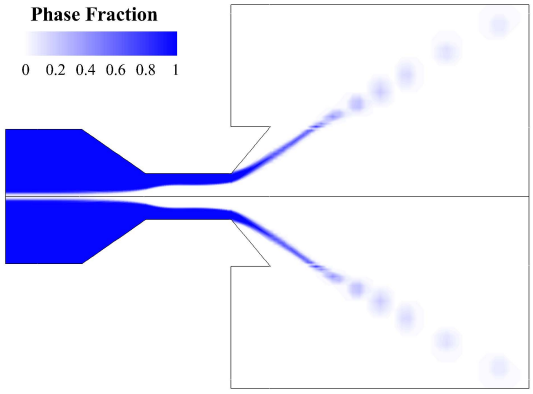

Figure 8. Instantaneous phase contour of atomizer internal flow

tics, 20,000 individual drops were recorded at each measurement location. Data rates (20-4300 Hz) and spherical validation values (90 - 100 %) varied depending upon the operating conditions and measurement locations.

High speed visible imaging is used to visualize the spray. A high-speed visible camera (Vision Research Phantom v7) with a 105 mm lens was mounted perpendicular to the spray axis, and a 150 W light source and diffuser plate were positioned behind the spray to provide backlighting. The spatial resolution of the visible intensity measurements was 167 μm for each pixel at the center of the spray. The visible camera integration time (20 μs) and aperture size ($f/22$) were selected to optimize the camera sensitivity.

For the spray measurements, the uncertainty in measurement location in the spray was approximately $\pm$ 1 mm for both axial and radial traverses. The fuel flow rate was measured across a choked venturi of known co-efficient of discharge. The uncertainty in measurement in the flow rate of fuel was at most 3%. The flow rate of air was set based on pressure drop across the pressure swirl atomizer. This measurement was made using a differential pressure gauge with an uncertainty of 0.12 psid.

Model Combustor and Experimental Setup

A single element Lean Direct Injection (LDI) combustor developed to characterize combustion dynamics in a multiphase combustion environment at high pressure ($\sim$1 MPa) has been used in this study. The combustor operates with Jet-A as the fuel and heated air (up to 800 K) air as the oxidizer. The combustor is designed in a modular configuration so that various lengths of the air plenum section and combustion chamber section can be utilized to tune the combustor dynamics to different pressure fluctuation amplitudes and frequencies. Figure 6 shows a schematic diagram of the combustor.

In the combustor, heated air passes through a helical vane swirler (60° vane angle) before being accelerated into the combustion chamber via a subsonic converging diverging venturi. The swirler has six helical vanes and is fixed to the fuel injector as shown in Fig. 7. The fuel is injected into the combustor using a pressure swirl atomizer. The inlet section of the combustion chamber has a thermal barrier coating applied to it to avoid heat loss through the walls and provide a near adiabatic boundary condition. This allows for better comparison with computational results where an adiabatic wall boundary condition is employed. The combustion chamber has a choked exit orifice that sets the chamber pressure in the combustor. Choked inlet and exit orifices on the combustor help set a closed acoustic boundary condition. Major operation parameters and design envelop are summarized in Table 1.

Comprehensive fuel spray modeling and measurements

The fuel spray model begins with the atomizer internal flow analysis as indicated in Fig. 8. This analysis is based on an Eulerian VOF method and is conducted independent of the Lagrangian spray simulations. The liquid fuel is supplied into the atomizer through two inlet ports located in the downstream section of the vortex chamber. A gas core is observed to exist in the center of the chamber due to the centrifugal force of the liquid fuel. About one diameter away from the orifice exit, the liquid sheets are dynamically disintegrated into droplets.

Liquid sheet data at the orifice exit plane is investigated to define the spray injection in the Lagrangian simulation. The sheet thickness, spray angle and velocity are used to describe the initial drop size, drop injection angle and speed respectively.

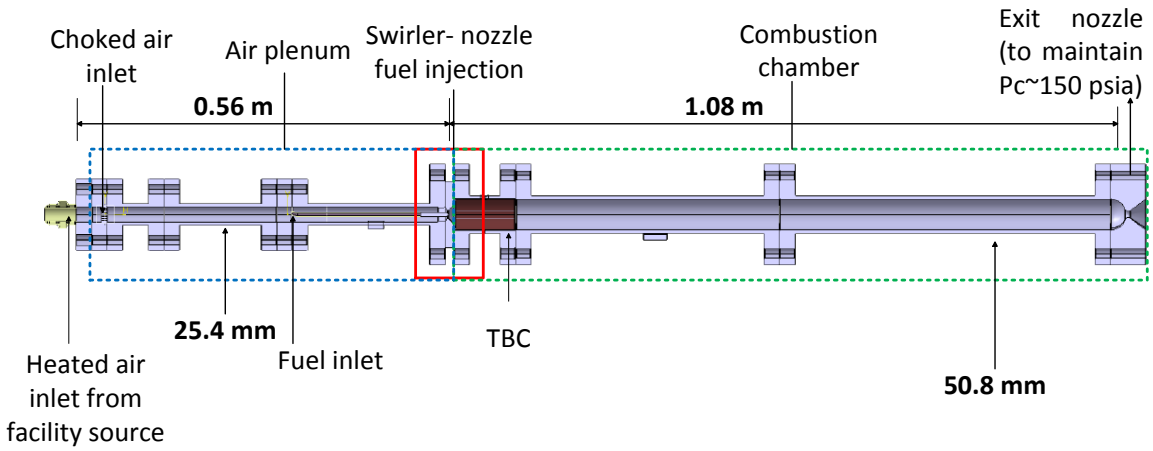

Figure 6. Schematic diagram of the experimental arrangement of the LDI combustor

Table 1. Summary of design envelope and nominal operation parameters

Fuel	-	Jet-A/JP8
Oxidizer	-	Air
Inlet Air Temperature	(K)	750 (nominal)
Equivalence Ratio	-	0.6 (nominal)
Frequency	(Hz)	400
Inlet Boundary Condition	-	Constant mass inflow
Exit Boundary Condition	-	Choked nozzle
Diameter of combustor	(mm)	50.8
Diameter of air plenum section	(mm)	25.4

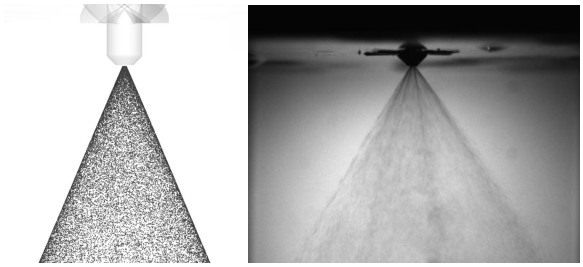

Figure 9. Snapshot from the fuel spray simulation (left) and high speed camera image (right) for the spray without co-flowing air

$\dot{m}_f$ (g/s)	Φ	θ (°)
2.27	0.4	70
2.84	0.5	69
3.41	0.6	68

Table 3. Measured Spray Angles

These variables are investigated in terms of fuel mass flow rates within the operating range (Φ = 0.4, 0.5 and 0.6). Results are summarized in Table 2.

Spray without co-flowing air

The fuel spray injected by the pressure swirl atomizer in the LDI element is modeled for the condition without co-flowing air at atmospheric pressure. Hollow cone injection of the spray is assumed for the injection conditions obtained from Table 2. For example, for an equivalence ratio of 0.6 ($\dot{m}_f$ = 3.41 g/s), an initial drop size of 78 μm is assumed and the drops are randomly distributed in the azimuthal direction. These initial spray drops are injected from the nozzle tip at 52.4 m/s with a 32 degree inclined angle measured from the nozzle axis. A snapshot from the simulation and the high speed camera image taken from the experiment are shown in Fig. 9. The measured spray cone angles are investigated with respect to the flow conditions in Table 3. The computational results of the spray cone angles show good agreement (within 6 %) with the experimental results based on image data.

Drop size distribution and axial velocity profiles based on the PDA measurements are presented in Figs. 10 and 11 respectively. The measurements have been conducted at multiple radial locations in the spray at three axial planes. The z-direction in the figures is the axial direction of the spray with the origin being located at the exit tip of the atomizer. The drop-sizes characterized by the Sauter mean diameter (SMD or D_{32}) lie between 20-50 μm. The maximum drop size is observed in the center at the maximum axial distance, Z = 44.45 mm, and can

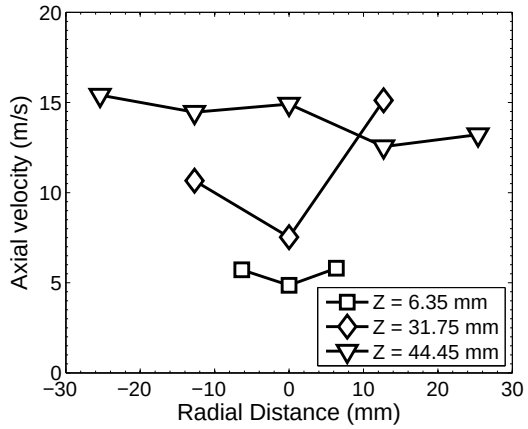

Figure 10. SMD results for the spray without co-flowing air

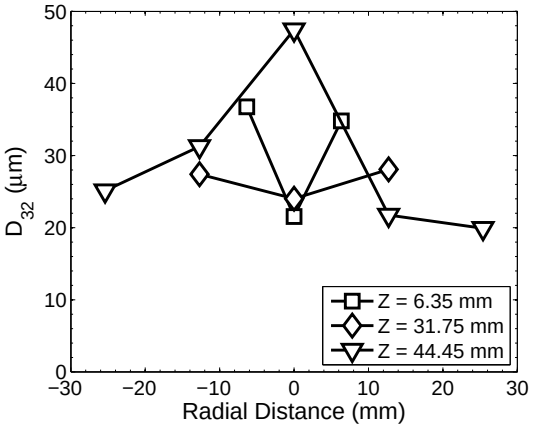

Figure 11. Axial velocity profiles for the spray without co-flowing air

be attributed to droplet coalescence. We note that the predicted drop sizes are larger than the measured drop sizes. The initial drop size estimated by Ibrahim and Jog's model is 77 μm. It may be anticipated that, if this predicted size is correct, then the drops would need to be atomized by the secondary breakup process. However, the secondary atomization process in the present simulation does not seem to be appropriately described by the K-H instability model and no secondary atomization is predicted. As shown in Fig. 11, axial velocities are observed to be higher as the spray travels further downstream implying acceleration of the drops in the spray. This acceleration may be associated with a complicated atomization process that is not predicted by the KH model.

Table 2. Orifice exit flow conditions

$\dot{m}_f$ (g/s)	Φ	V_r (m/s)	V_θ (m/s)	t (μm)	θ (deg)	$\|\mathbf{V}\|$ (m/s)
2.27	0.4	1.94	30.46	77	66	37.1
2.84	0.5	2.43	38.07	77	65	44.2
3.41	0.6	2.91	45.69	78	64	52.4

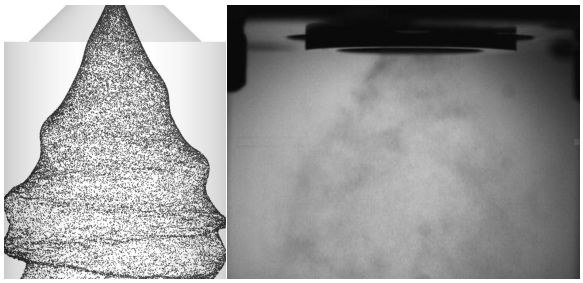

Figure 12. Snapshot from the fuel spray simulation (left) and high speed camera image (right) for the spray with co-flowing air

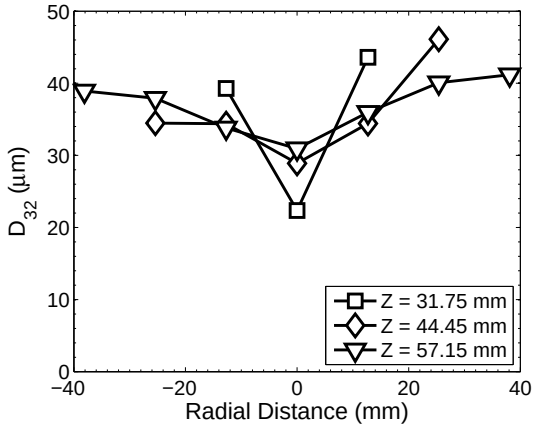

Figure 13. SMD results for the spray with co-flowing air

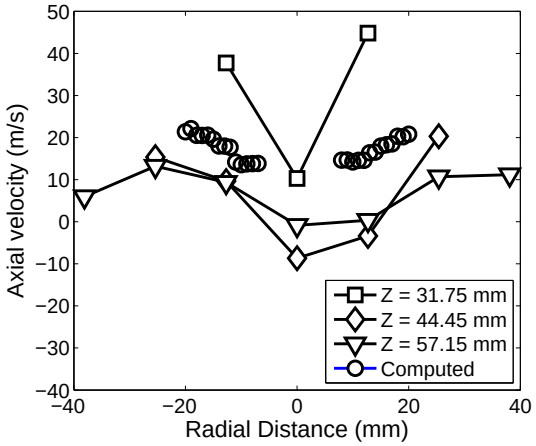

Figure 14. Axial velocity profiles for the spray with co-flowing air

Spray with co-flowing air

The fuel spray modeling and experiments are next shown for the condition with co-flowing air. In the simulation, the spray cone is spirally distorted and spins along the injector axis on account of strong interaction with the co-flowing air as shown in Fig. 12. This dynamic motion is also observed in the experiment. The high speed camera image is taken right after the venturi end and visualizes the spinning spray cone. The fuel injector tip is located approximately 15 mm upstream of the venturi exit.

Drop size distribution and axial velocity profiles for the spray with co-flowing air are presented in Figs. 13 and 14. It is important to note that the axial slices at which measurements were made are different than the case with no co-flowing air. This is on account of not being able to access the region covered by the venturi. The overall level of drop size for the spray with co-flowing air is between 30-40 μm. The drop-sizes for axial locations 44.75 mm and 57.15 mm are of the same order. The drop-size immediately downstream of the nozzle is smallest ($\sim$20 μm). The axial velocity of the co-flowing air may contribute to reducing the relative velocity between spray drops and gas so that the larger drops are produced particularly away from the center. As indicated, larger axial velocities are observed at the near-nozzle plane, Z = 31.75 mm, in Fig. 14. It is also noteworthy to observe the backflow in the middle at Z = 44.75 and 57.15 mm. The swirl number of the jet in this experimental set-up is approximately 0.8. For such high swirl numbers, a central toroidal recirculation zone (CTRZ) is commonly observed on account of adverse axial pressure gradients exceeding the inertial forces of droplets and leading to flow reversal [2]. Finally, we also note that the computed results in Fig. 14 show axial velocities in the range of 10-30 m/s.

Effect of the fuel spray modeling on the chamber acoustics

The chamber acoustics driven by combustion are studied in a series of combustion dynamics simulations with fuel spray modeling. The three distinct fuel spray modeling methods indicated in Table 4 are used. In Case 1, the spray drops are injected using a log-normal size distribution satisfying a given fuel flow rate. No secondary atomization process is described in this case. Case 2 assumes large single drop injection with the drop size being the same as the order of orifice diameter (= 300 μm). For this drop size, secondary atomization occurs as soon as the drop is injected into the chamber. Case 3 is the fuel spray modeling method used for the non-reacting spray simulations with and without co-flowing air. It is the most realistic spray model for the pressure swirl atomizer. This fuel spray model uses the initial drop size and injection velocity obtained from the Eulerian VOF calculation as described earlier.

The spray formation and corresponding heat release pattern are visualized in Fig. 15 for the three cases. In all cases, the fuel sprays are almost entirely consumed prior to the combustor head region itself. In particular, Cases 1 and 2 indicate complete fuel consumption before drops reach the combustor head. In Case 3, the spray cone penetrates one chamber radius downstream and shows a spiral surface wave that is driven by the swirling air. The larger momentum of drops in Case 3 seems to lead to the longer spray penetration. We note that this case also corresponds to the situation where the KH model does not predict secondary atomization which may further explain why the drops last longer. In addition to the spray penetration, the spray pattern can also be characterized distinctly for the three cases. Case 1 exhibits more-or-less regularly distributed drops within a solid cone. The vaporization process occurs over the entire spray cone including the cone axis. Case 2 shows strong secondary atomization process in the venturi diverging section. The rim of the spray cone is the location where the secondary atomization and the resulting vaporization seems to occurs. In Case 3, few spray drops are located along the cone axis due to the hollow cone injection. The fuel spray is spirally supplied into the chamber and the vaporization occurs at the end of spray cone.

The heat release is distributed corresponding to the spray cone formation and drop distribution. Strong reaction and heat release occur in the venturi diverging section for all cases, but the heat release pattern in the combustor beyond the venturi depends upon the fuel spray model. In Case 1, the reactions take place strongly even in the central zone of the combustor head. Case 2 shows strong heat release along the rim of the spray cone and it continues near the combustor wall. Case 3 has a more stretched flame zone than Case 2 and the strong heat release seems to follow the pattern of flow separation at the walls.

Peak-to-peak pressure amplitudes of the combustor wall pressure are investigated for the three simulation cases and are summarized in Table 5 along with the measured experimental result. The table also shows the dominant acoustic mode in each case. The experiment indicates an amplitude that is 5% of the mean pressure which seems to be within the range that other researchers have reported [3]. The computed pressure amplitudes, on the other hand, are a strong function of the fuel spray model. The log normal drop injection method (Case 1) gives the largest pressure amplitude (11%), the single drop injection method (Case 2) produces a similar level of pressure amplitude (7%) as the experiment, and the hollow cone injection method (Case 3) indicates a much lower pressure amplitude (0.24%). It is noteworthy that Case 3 predicts the correct instability mode compared with the experiment (4L).

The power spectrum density (PSD) analysis of the wall pressure provides the dominant acoustic modes in each case as shown in Fig. 16. The PSD based on the experimental results indicates the 4L mode as the dominant frequency (1425 Hz). We note that this frequency is lower than the designed 4L frequency of 1600 Hz because the combustor dimensions were determined based on adiabatic and complete combustion. As noted earlier, the dominant acoustic modes are observed to be different for each case. The log normal drop injection case (Case 1) predicts a dominant 1L frequency. The single drop injection case (Case 2) predicts a dominant 2L frequency. The hollow-cone case (Case 3) predicts the 4L mode which is in agreement with the experimental mode.

Furthermore, it is noteworthy that the broad-frequency-range PSD in Case 3 is also qualitatively similar to that of the experimental result as seen in Fig. 17, although the peak strengths are very different. In addition to the 4L mode at 1425 Hz, the other distinct frequencies observed are 3000, 6000 and 9500 Hz. Hydrodynamic instability (or the so-called precessing vortex core instability) drives the 3000 and 6000 Hz modes and the tangential acoustic mode is observed at 9500 Hz.

Label	Injection Method	D μm	$\|\mathbf{V}\|$ (m/s)	Secondary Atomization
Case 1	Log Normal Distributed Drop Injection	1-100	30.0	X
Case 2	Single Drop Injection	200	30.0	O
Case 3	Hollow Cone Injection	78	52.4	O

Table 4. Summary of fuel spray modeling in combustion dynamics simulations

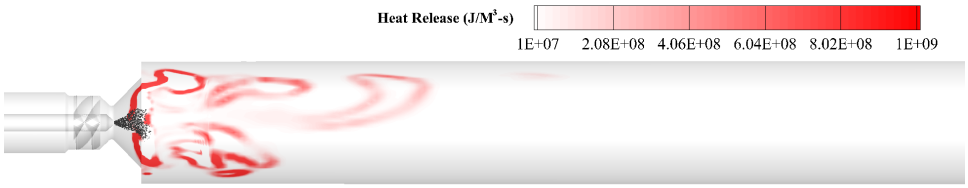

(a) Case 1: Log-normal distributed drop injection

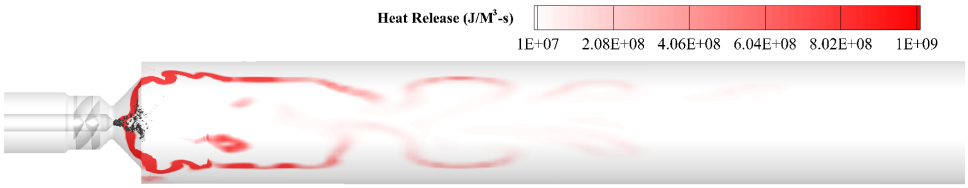

(b) Case 2: Single drop injection

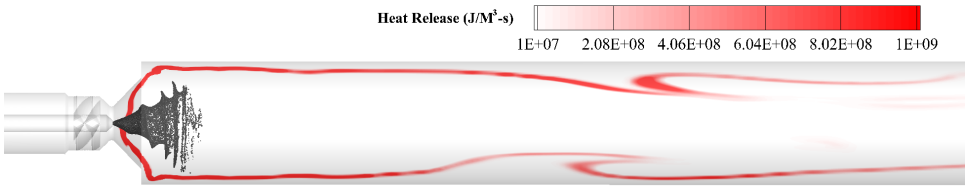

(c) Case 3: Hollow cone injection

Figure 15. Instantaneous heat release contours in terms of fuel spray modeling

Discussion

Experimental Uncertainty Factors

The spray from the pressure swirl atomizer was characterized using PDA and high speed videos. All the measurements were performed at atmospheric pressure and temperature in an unconfined flow. Measurements with an optically accessible polycarbonate cylindrical section with dimensions similar to the combustor were attempted. Good quality data could not be obtained in these measurements on account of fuel film formation on the surface of polycarbonate section, even with a co-flow of air. The PDA measurements yielded drop-sizes between 20 to 50m depending on location in the spray and fuel flow rate. The drop-sizes are also dependent on the co-flow of air around the fuel injector. The effect of CTRZ is evident in the drop-sizes and the axial velocities measured in the spray, especially beyond a distance of approximately 44 mm from the atomizer exit. For the case with a co-flow of air measurements were only possible at locations 44 mm and further downstream of the atomizer on account of the presence of the subsonic venturi which impeded optical access. The high speed videos of the spray were used only for the determination of the spray cone angle and for a qualitative comparison of the overall spray behavior with computational data. Further studies would include optical patternation measurements to calculate mass flux density of the spray along multiple axial slices.

For the spray measurements, the uncertainty in measurement location in the spray was approx-

Cases	Peak-to-Peak Pressure Oscillation Amplitude (%)	Dominant Acoustic Mode
Experiment	5	4L
Case 1: Log Normal Distributed Drop Injection	11	1L
Case 2: Single Drop Injection	7	2L
Case 3: Hollow cone injection	0.24	4L

Table 5. Summary of pressure oscillations in a longitudinal mode

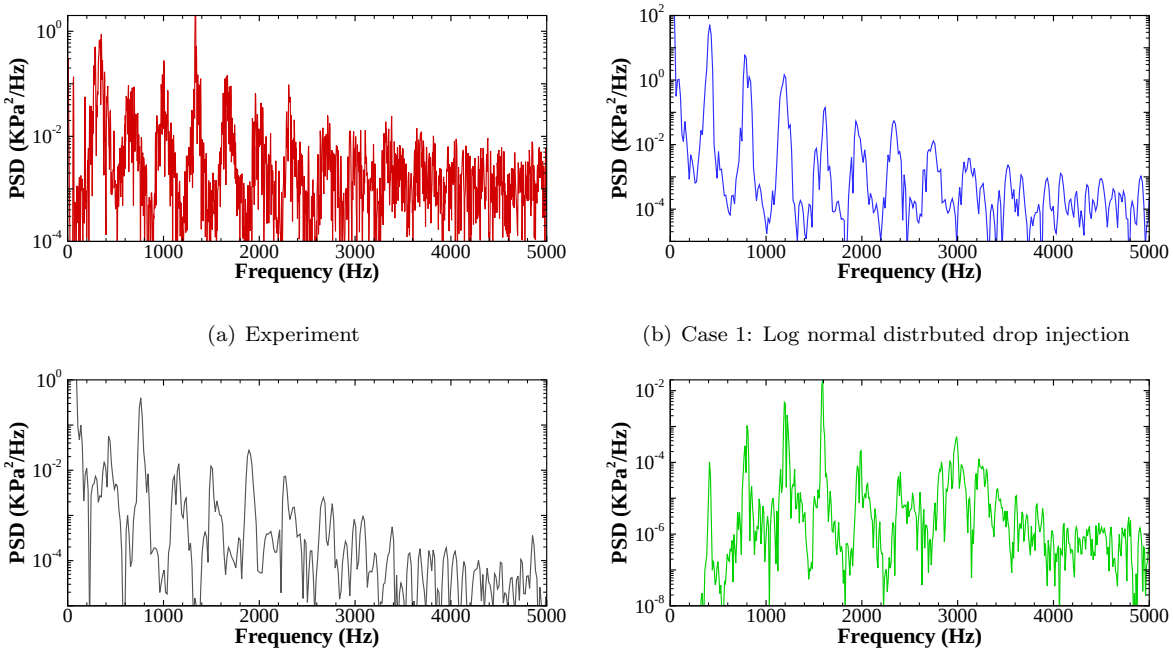

(a) Experiment

(b) Case 1: Log normal distrbuted drop injection

(c) Case 2: Single drop injection

(d) Case 3: Hollow cone injection

Figure 16. PSD results from the experiments and simulations

imately ±1 mm for both axial and radial traverses. The fuel flow rate was measured across a choked venturi of known co-efficient of discharge. The uncertainty in measurement in the flow rate of fuel was at most 3%. The flow rate of air was set based on pressure drop across the pressure swirl atomizer. This measurement was made using a differential pressure gauge with an uncertainty of 0.12 psid.

Limitations of KH Breakup Model

Non-reacting spray simulations with and without co-flowing air indicated limitations in the prediction of drop size distributions. This may be attributed to the insufficient representation of the secondary atomization in the Kelvin-Helmholtz instability model. This model is based on the linear stability analysis subject to the velocity difference between liquid and gas. In this respect, the Weber number is a key factor for the KH breakup. Weber numbers over the spray cone were lower than the critical Weber number ($We_c = 12$) for KH breakup because of the fine drop size resulting from the primary atomization model. The small drop sizes of about 70 μm results in a weak aerodynamic force, which is not enough to drive KH breakup.These results indicate that an alternate breakup model could be used to describe the secondary atomization for drop sizes less than 100 μm. The Rayleigh-Taylor (RT) breakup model which is driven by droplet acceleration would be an ideal candidate for this, particularly given the low Weber numbers. Future work will consider augmenting the secondary atomization process with the RT model.

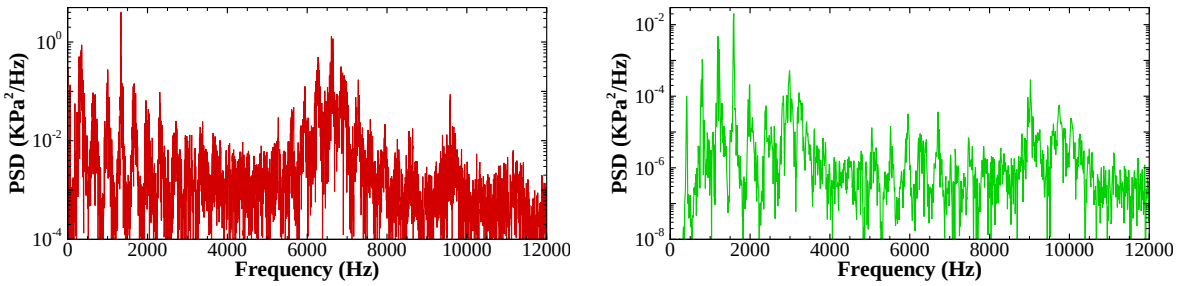

(a) Experiment

(b) Case 3: Hollow cone injection

Figure 17. Broad range PSD results

Impacts of the fuel spray modeling on self-excited combustion instabilities

According to the combustion dynamic simulation results, the chamber acoustics are strongly influenced by the fuel spray modeling. It can be analyzed in terms of the frequency and amplitude characteristics. First, only the simulation using the hollow cone injection indicated the 4L mode dominant acoustic frequency corresponding to the experimental result. In this case, stronger drop momentum and fine drop sizes are observed, resulting from the atomizer internal flow analysis. Moreover, as noted earlier, the KH model does not predict secondary atomization for the fine drop sizes. As a result, the fuel spray cone penetrates deeply into the combustion chamber, and the flame is distributed along the combustor wall. Such a fuel spray and heat release pattern may be responsible for triggering the higher acoustic mode since this has a pressure anti-node that is located close to the downstream heat release location.

The pressure amplitude from the simulation using hollow cone injection is the most underestimated result among all cases. This can be accounted for by the insufficient description of the secondary atomization process. The small acoustic perturbation seen here is driven by the relatively weak strength of highly distributed heat release pattern. We note that the secondary atomization typically enhances the vaporization rate by increasing the surface area of the drops. Hence, the absence of significant secondary atomization seems to result in low vaporization rates which in turn lead to a distributed and weak heat release and, consequently, to low pressure amplitudes. As observed earlier, better secondary atomization modeling is needed to obtain more quantitatively accurate predictions of the pressure amplitudes.

Conclusion

This study has focused on the fuel spray modeling and its impact on chamber acoustics in combustion dynamics simulations. The fuel spray model is comprehensively described by sub-models for the atomizer internal flow, hollow cone injection and secondary atomization. To validate the model and to guide its further development, the fuel spray modeling is exercised for non-reacting spray conditions with and without co-flowing air. Corresponding spray measurements have been performed using PDA and high speed image camera.

The spray angle from the simulation results agrees with that from the experiment to within 6% error. According to the drop size distributions measured, it is found that Kelvin-Helmholtz model in the LDI spray does not sufficiently describe the secondary atomization given the fine drop sizes that are predicted by the primary atomization process. The spray measurements with co-flowing air indicate negative velocities in the center of chamber which confirms the presence of the CTRZ structure.

Three fuel spray models are compared in the combustion dynamics simulations to investigate the effects on chamber acoustics driven by thermoacoustic instabilities. The models are characterized by the injection methods as log normal distributed drop, single drop and hollow cone injection. The fuel spray described by the hollow cone injection is most advanced and realistic choice. Using the hollow cone injected sprays, the 4L mode dominant acoustic frequency is obtained which is in good agreement with the experiment. On the other hand, the corresponding pressure amplitudes are underestimated. Again, this discrepancy may be attributed to insufficient secondary atomization and the resultant low vaporization rates. Future work will concern the addition of the Rayleigh-Taylor breakup model to better describe these phenomena.

Acknowledgment

The authors acknowledge the support of the NASA Glenn Research Center under NASA Research Announcement (NRA) grant number NNX11AI62A, with Program Manager Kimlan Phan and Technical Monitor Kevin Breisacher. Also, we would like to give special thanks to Drs. Charles Merkle and Hukam Mongia who set the original direction of the study, Dr. Guoping Xia in the United Technology Research Center for the contribution of the initial computational model used in this study, and Mr. Phil Lee of Woodward for providing the fuel nozzle used in the experiment. The help of Prof. Sojka and Varun Kulkarni with the PDA experiment and overall guidance is also greatly appreciated.

Nomenclature

a	parent drop radius
d	drop diameter
m	mass
r	child drop radius
t	time
$\dot{m}$	mass flow rate
A	Area
B	KH breakup mode constant
N	Number
P	pressure
U	drop speed
V	velocity or gas velocity
FN	Flow number
Oh	Ohnesorge number
Ta	Taylor number
We	Weber number
λ	wave length at maximum growth rate
ν	viscosity
Ω	the maximum growth rate
Φ	Equivalence ratio
ρ	density
σ	surface tension
θ	inclined angle of drops

Subscripts

f	fuel
g	gas
l	liquid
s	slot
r	radial
θ	tangential
0	previous time step

References

[1] R. Tacina. Low NOx Potential of Gas Turbine Engines *In 28th AIAA Aerospace Sciences Meeting and Exhibit*, Reno, Nevada, Jan. 1990. AIAA 1990-0550.

[2] Y. Fu, S. Jeng, and R. Tacina. Characteristics of the Swirling Flow in a Multipoint LDI Combustor *In 45th AIAA Aerospace Sciences Meeting and Exhibit*, Reno, Nevada, Jan. 2007.

[3] Y. Tongxun and D. A. Santavicca. *Journal of Propulsion and Power*, 25(5):1058–1067, 2009.

[4] C. Yoon, R. Gejji, W. Anderson, and V. Sankaran. Computational Investigation of Combustion Dynamics in a Lean Direct Injection Gas Turbine Combustor *In 51st AIAA Aerospace Sciences Meeting including the New Horizons Forum and Aerospace Exposition*, Grapevine, TX, Jan. 2013.

[5] M. Jog S. Jeng and M. Benjamin. *AIAA Journal*, 36(2):201–207, 1998.

[6] J. Cousin, S.J. Yoon, and C. Dumouchel. *Atomization and Sprays*, 6:601–622, 1996.

[7] N. Patel and S. Menon. *Combustion and Flame*, 153(1-2):228–257, 2008.

[8] R. Reitz. *Atomisation and Spray Technology*, 3:309–337, 1987.

[9] M. Patterson and R. Reitz. Modeling the Effects of Fuel Spray Characteristics on Diesel Engine Combustion and Emission, Jan. 2007. SAE 980131.

[10] D. Dewanji, A. G. Rao, M. Pourquie, and J. V. Buijtenen. Simulation of Reacting Spray in a Multi-Point Lean Direct Injection Combustor *In 48th AIAA/ASME/SAE/ASEE Joint Propulsion Conference and exhibit*, Atlanta, GA, July 2012. AIAA 2012-4324.

[11] H. El-Asrag, F. Ham, and H. Pitsch. Simulation of a lean direct injection combustor for the next high speed civil transport (hsct) vehicle combustion systems, 2007.

[12] J.M. Senoner, M. Sanjose, T. Lederlin, F. Jaegle, M. Garcia, E. Riber, B. Cuenot, L. Gicquel, H. Pitsch, and T. Poinsot. *Combustion for aerospace propulsion*, 337(6-7):458 – 468, 2009.

[13] D. Li, G. Xia, V. Sankaran, and C. L. Merkle. Computational Framework for Complex Fluids Applications *In 3rd International Conference on Computational Fluid Dynamics*, Toronto, Canada, July 2004.

[14] R. A. Baurle et al. *AIAA J.*, 41(8):1463–1480, 2003.

[15] A. Travin et al. *Advances in LES of Complex Flow, Fluid Mechanics and Its Applications*, 65:239–254, 2004.

[16] D. Basu et al. DES, Hybrid RANS/LES and PANS Models for Unsteady Separated Turbulent Flow Simulations *In ASME 2005 Fluids Engineering Division Summer Meeting*, pp. 683–688, Houston, TX, 2005.

[17] C. K. Westbrook and F. L. Dryer. *Combustion Science and Technology*, 27, 1981.

[18] A. A. Ibrahim and M. A. Jog. *Journal of Engineering for Gas Turbine and Power*, 129(4):945–953, 2007.